IEEE Photonics Journal
An IEEE Photonics Society Publication

The Simulation of Vortex Modes in Twisted Few-Mode Fiber With Inverse-Parabolic Index Profile

Volume 12, Number 3, June 2020

Zhiming Zhang
Xiuying Liu
Wei Wei
Lei Ding
Liqing Tang
Yigang Li

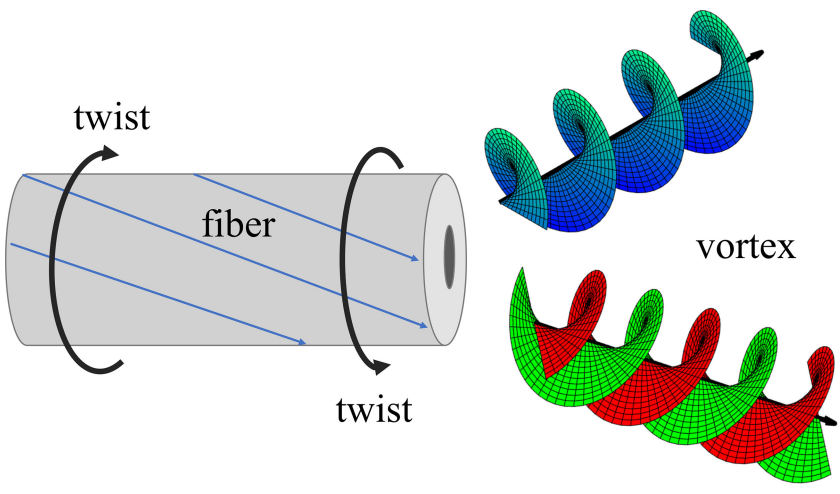

DOI: 10.1109/JPHOT.2020.2994819

The Simulation of Vortex Modes in Twisted Few-Mode Fiber With Inverse-Parabolic Index Profile

Zhiming Zhang, Xiuying Liu, Wei Wei, Lei Ding, Liqing Tang, and Yigang Li

School of Physics, Nankai University, Tianjin 300071, China

DOI:10.1109/JPHOT.2020.2994819

Manuscript received April 12, 2020; revised May 6, 2020; accepted May 11, 2020. Date of publication May 14, 2020; date of current version May 26, 2020. This work was supported in part by the National Key R&D Program of China (2017YFA0303800), in part by the National Natural Science Foundation of China (No. 11474170), and in part the Natural Science Foundation of Tianjin, China (No. 16JCYBJC16900). Corresponding authors: Lei Ding and Yigang Li (e-mail: dinglei@nankai.edu.cn; liyigang@nankai.edu.cn).

Abstract: The eigenmodes of an inverse-parabolic graded index fiber under torsion were investigated by using the finite element method simulation. These eigenstates correspond to orbital angular momentum modes except for the two polarized-vortex modes. The design of appropriate core parameters can lead to the difference in the effective refractive indexes between all adjacent modes being greater than 10^{-4} over a bandwidth of 1.5 to 1.6 μm, which is expected to be an ideal method for the generation of multiple vortex modes in few-mode fiber for optical communication. The results showed that the separation of these modes changes with twist rate. Compared to the twisted air-hole ring-core fiber, the optimal twist rate of this fiber was found to be an order of magnitude smaller, which provides a more feasible scheme for the combination of mode division multiplexing and wavelength division multiplexing. We speculate that this study may have promising prospects in various applications such as particle manipulation, imaging, and quantum communication.

Index Terms: Eigenmode, fiber, vortex mode.

1. Introduction

With increasing demand for effective optical communication capacity, single-mode optical fibers meet a bottleneck for their implementation in quantum communication [1]. Therefore, mode division multiplexing may be an effective approach to solve this problem [2]. The vortex beam is expected to be used in future communication systems due to its orbital angular momentum (OAM) [3], [4]. The order of the optical OAM is represented by the topological charge, and vortex beams with different topological charges are orthogonal. Although the initial experiment using optical OAM for communication was carried out in free space [5], the limited propagation distance restricted its further development. Fiber has undoubtedly become the backbone of communication systems. Therefore, generation and propagation of a vortex beam in an optical fiber has become an important research topic. Furthermore, beams with well-defined optical OAM have found many interesting applications including particle manipulation and trapping [6], [7], quantum computing [8], and quantum communication [9]. Multimode fiber supporting the OAM mode was first proposed by Alexeyev *et al.* in 1998 [10]. A decade later, the first experiment about OAM data transmission

was demonstrated in a special-designed fiber [11]. Subsequently, an air-core fiber and an inverse parabolic graded index fiber were designed to support 3 OAM orders for a total of 12 states, and 2 OAM orders for a total of 8 states, respectively [12], [13]. A ring-index photonic crystal fiber for the delivery and nonlinear optical interactions of OAM modes was also reported [14].

However, the above mentioned studies and most of the current studies on generation of a vortex beam in the fiber depend on the superposition of eigenmodes [15] or the superposition of scalar modes, as shown below

$$\begin{aligned} &OAM_{\pm l,m} = LP^{a}_{l,m} \pm \boldsymbol{j} \cdot LP^{b}_{l,m} \qquad (a) \\ &OAM^{\pm}_{\pm l,m} = HE^{even}_{l+1,m} \pm \boldsymbol{j} \cdot HE^{odd}_{l+1,m} \quad (b) \quad \text{(sign of OAM and SAM is the same)} \\ &OAM^{\mp}_{\pm l,m} = TM_{0,m} \pm \boldsymbol{j} \cdot TE_{0,m} \quad (l=1) \quad (c) \\ &OAM^{\mp}_{\pm l,m} = EH^{even}_{l-1,m} \pm \boldsymbol{j} \cdot EH^{odd}_{l-1,m} \quad (l>1) \quad (d) \end{aligned} \Bigg\} \text{(sign of OAM and SAM is the opposite)} \qquad (1)$$

The orbital angular momentum mode is denoted as $OAM^{\pm}_{\pm l,m}$, where l represents the topological charge and m denotes the number of concentric rings of the pattern. The sign of the superscript indicates left- or right-circular polarization, and the symbol of l represents the direction of rotation of the wavefront [16]. Noteworthy, there must be a phase difference of $\pi/2$ between the two coherent superposition modes, and $\boldsymbol{j}$ represents the $\pi/2$ phase.

Expression (1-a) indicates that two scalar modes generate a vortex mode, and each scalar mode includes a pair degenerate eigenmodes, and this results in low utilization of the modes. In order to make (1-b), (1-c), and (1-d) available, it is necessary to use some means to lift the degeneracy among the degenerate scalar modes, such as polarization effects, bending of the optical fiber or the elliptical core [16], [17]. The eigenstates in a twisted fiber also correspond to vortex beams. Ye *et al.* proposed the use of twisted fiber with a ring core and an air hole to make the effective index difference between adjacent vortex eigenmodes greater than 10^{-4}; however, the twist rate they applied was so high that it was difficult to realize in practical applications [19].

In this study, a twisted fiber with an inverse-parabolic index profile was proposed, and the eigenmodes of this fiber were simulated by using the finite element method involving the use of theoretical simulation software, namely, COMSOL5.4. Compared to the twisted air-hole ring-core fiber [19], the optimal twist rate of the proposed fiber was an order of magnitude smaller which naturally resulted in less torsional stress. Its center is solid, unlike air-hole ring-core fiber, thus it is easier to weld with other fibers.

2. Related Theories and Parameters

The distribution of the refractive index along the radius of the fiber can be described by using the following formula:

$$n(r) = \begin{cases} n_1\sqrt{1 - 2N\Delta\left(\frac{r}{r_0}\right)^2}, & 0 \le r \le r_0 \\ n_2, & r > r_0 \end{cases} \qquad (2)$$

where n_1 and n_2 are the core refractive index and the cladding refractive index, respectively. The curvature factor $N = (n_1 - n_a)/(n_1 - n_2)$, $\Delta = ({n_1}^2 - {n_2}^2)/2{n_1}^2$ is the relative refractive index difference, and n_a represents the refractive index value at the interface between the core and the cladding [20]. In this study, various parameters are as follows: $n_1 = 1.454$, $n_2 = 1.444$, $n_a = 1.55$, $N = -9.6$, and $r_0 = 5.5\ \mu m$. The refractive index distribution is shown in Figs. 1(a) and (b).

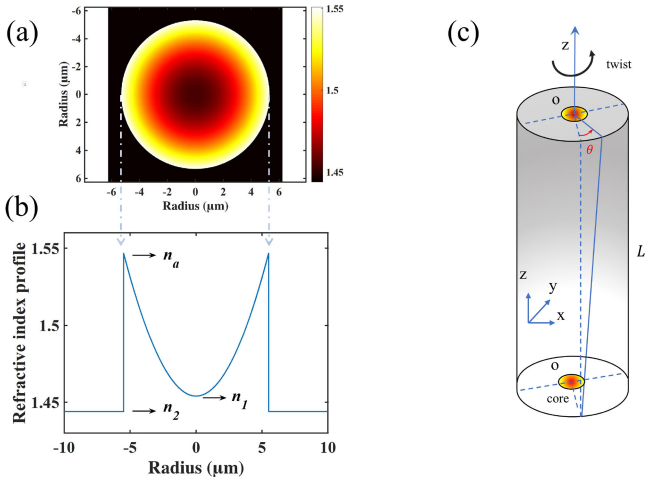

Fig. 1. (a) and (b) Cross section of inverse-parabolic index fiber and its index profile and (c) Schematic illustration of geometry of twisted inverse-parabolic index fiber

Under torsional stress, the refractive index distribution of the fiber is anisotropic [19], [21]–[23]. The dielectric constant is a tensor, expressed as follows:

$$\varepsilon' = \begin{bmatrix} \left(1+(p\alpha)^2y^2\right)\varepsilon & -(p\alpha)^2xy\varepsilon & -p\alpha y\varepsilon \\ -(p\alpha)^2xy\varepsilon & \left(1+(p\alpha)^2x^2\right)\varepsilon & p\alpha x\varepsilon \\ -p\alpha y\varepsilon & p\alpha x\varepsilon & \varepsilon \end{bmatrix} \tag{3}$$

where ε is the dielectric constant of the material and α is the twisted rate, defined as the ratio of the twist angle to the length $\alpha = \theta/L$, as shown in Fig. 1(c). The cladding material was made up of quartz and core was doped with some elements to meet the changes in the refractive index. The photoelastic constant of quartz, p, is 35.7. Herein, x and y are Cartesian coordinates.

3. Simulation Results and Discussion

3.1 The Eigenmodes in the Vortex State

The number of modes and the degree of separation between modes are affected by the core radius. Too small core radius reduces the number of modes, and too large core radius leads to an m $>$ 1 mode (m $=$ 1 indicates that the intensity distribution of the mode is a single ring). The multi-ring intensity leads to the severe complications in multiplexing and demultiplexing of OAM, and also results in a crossing between effective indices of modes belonging to different mode groups, which is disadvantageous for inter-mode separation [24]. Considering the above mentioned factors, a core radius of 5.5 μm was selected, leading to a cladding diameter of 125 μm, and the twist rate of 33 rad m^{-1}. This design resulted in obtaining 22 eigenmodes in simulation. Out of 22 modes, 20 are OAM modes, all of which are circularly polarized. Two of the OAM modes are the fundamental modes which are different from those of the non-twisted few-mode fiber, and their intensity distribution is a doughnut shape rather than Gaussian distribution. In this way, the two fundamental modes can also be considered as OAM modes, except that their topological charges are zero, which is equally important in mode division multiplexing. In contrast, the other two linear polarized modes are non-orbital angular momentum modes. Their electric field distribution is the same as that of a transverse electric mode and transverse magnetic mode, which can be considered as a polarized-vortex mode. Moreover, the direction of the central electric field is uncertain, that is, there is an electric vector singularity, and thus all modes can be collectively referred to as vortex modes.

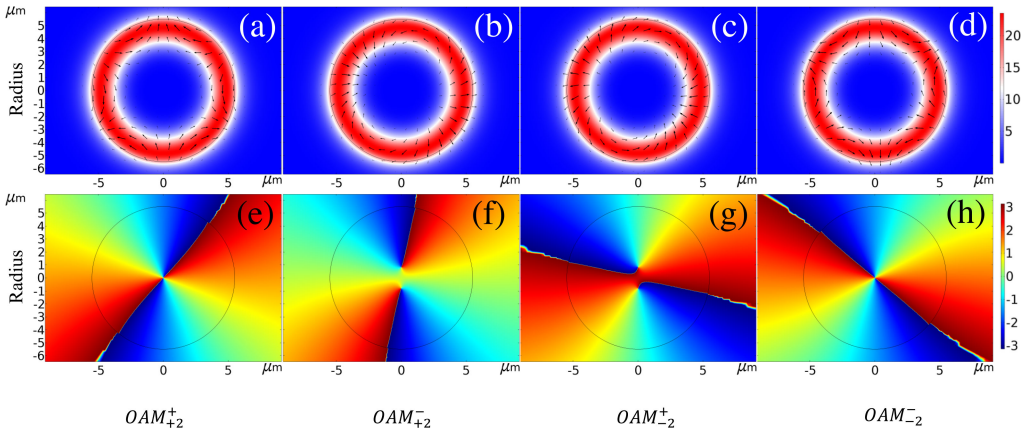

Fig. 2. (a–d) The direction (arrows) of transverse electric field and intensity of the guided vector modes in twisted inverse-parabolic index fiber with the following parameters: $\lambda = 1550$ nm and $\alpha = 33$ rad/m. (e–h) The phases corresponding to (a–d) modes. The dynamic images of the evolution of these vector vortex patterns over time (see supplementary materials)

The maximum topological charges of the 22 vortex modes reached 5. Considering the modes with topological charge of 2 (Figs. 2(a–d), the electric field distribution of these four OAM modes is the same as that of HE_{31} mode or EH_{11} mode, and their rotated wavefronts are indicated by their own vortex phase as shown in Figs. 2(e–f). The dynamic rotation of the electric field vector indicated that the polarization of the mode was left-handed or right-handed. The OAM of the four vortex modes was in the same or opposite direction as their own spin angular momentum, which is shown in terms of the evolution of the four vector vortex patterns over time (Fig. 2) (see supplementary materials).

3.2 The Effective Index Separation of Eigenmodes in Vortex State

The essential requirement of mode division multiplexing is that multimodes can be transmitted in a waveguide at the same wavelength. In contrast, wavelength division multiplexing requires that the modes with different wavelengths can be transmitted in a waveguide. The effective-index difference between adjacent modes can represent the effective-index separation between them. If the separation between modes is greater than 10^{-4}, crosstalk < -20 dB is possible [17]. Thus, the mode separation at different wavelengths was calculated herein. Fig. 3(a) shows the effective refractive indices of the 22 vortex eigenmodes with wavelengths ranging from 1.5 μm to 1.6 μm, exhibiting the separation of the modes from each other. In a conventional step-index fiber, the effective indices of the modes of the same mode group cannot be separated at this scale. Fig. 3(b) shows the effective refractive index difference between the adjacent modes. All the values are greater than 10^{-4}, with a minimum of 1.58×10^{-4}. This is presented in Fig. 3(c) where several lines in the lower part of Fig. 3(b) are magnified. This indicates that these vortex modes have a good separation at the given twist rate.

The anisotropic refractive index induced by torsion directly impacts the effective refractive index of the mode. The simulation shows that with the increase in the torsion rate, the effective refractive index of the 22 eigenmodes gradually move away from the initial value when the fiber is non-torsional (the twist rate is zero), as shown in Fig. 4(a). When the twist rate is higher than 100 rad m^{-1}, the effective refractive indices of some modes cross each other. When the twist rate is 105 rad m^{-1}, the phase of the vortex mode starts to become chaotic, as shown in Fig. 5(a). When the twist rate is 150 rad m^{-1}, the phase becomes completely disordered as shown in Fig. 5(b). Thus the

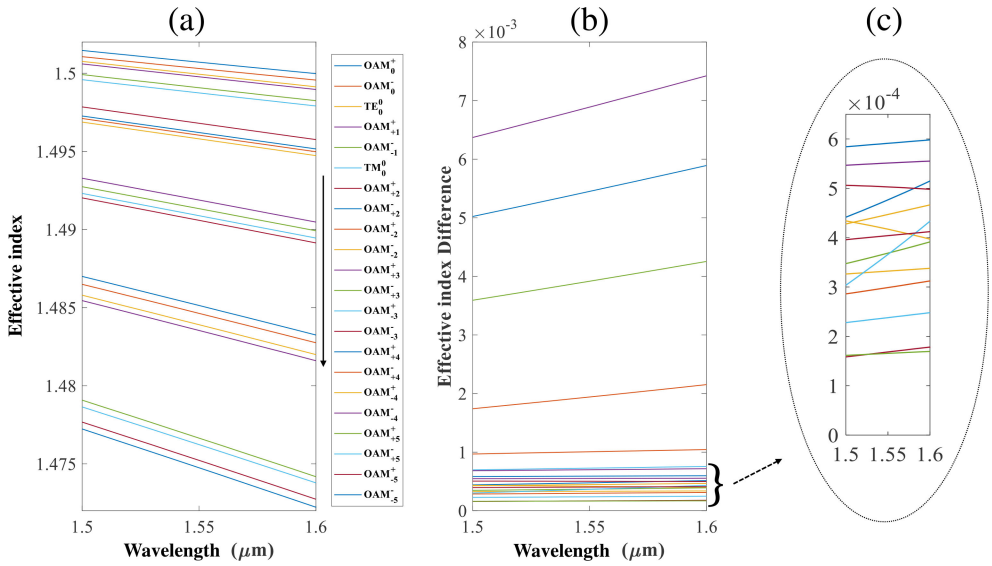

Fig. 3. (a) Effective indices and (b) Difference between the adjacent effective indices ($\Delta neff$) in (a) as a function of wavelength for eigenmodes in the twisted inverse-parabolic index fiber ($\alpha = 33$ rad/m). The mode represented by each line in (a) corresponds to the mode marked in the legend from top to bottom. (c) Zoom-in of the lower part of the (b)

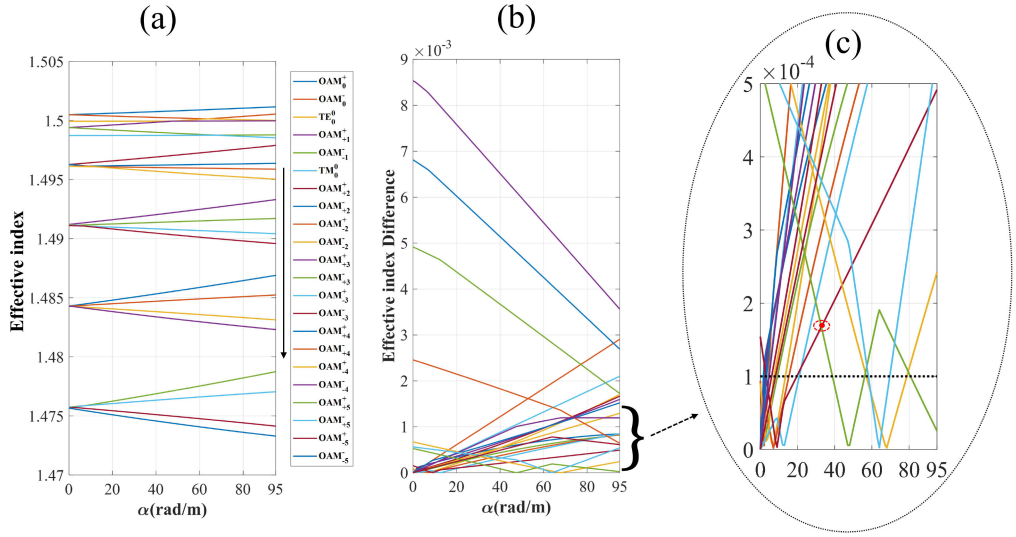

Fig. 4. (a) Effective indices and (b) Difference between the adjacent effective indices in (a) as a function of the twisted rate ($\lambda = 1550$ nm). The mode represented by each line in (a) corresponds to the mode marked in the legend from top to bottom. (c) Zoom-in of the lower part of the (b)

twist rate was calculated when the phases of modes with different topological charge started to be chaotic, as presented in the following Table:

Moreover, too high torsion rate leads to an increase in the difficulty of implementation; therefore, lower twist rates are desirable. Fig. 4(b) exhibits the difference in effective refractive indices of adjacent modes. This calculated value was used to identify twist rates that resulted in making all effective refractive index differences greater than 10^{-4}. Magnification of the bottom part of Fig. 4(b)

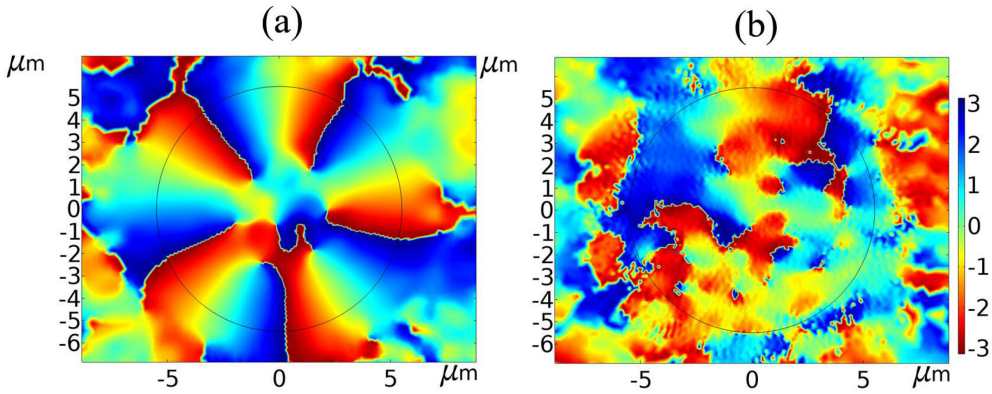

Fig. 5. The phase of the vortex mode OAM_{-5}^{-}: (a) when the twisted rate is 105 rad m^{-1} and (b) when the twisted rate is 150 rad m^{-1}.

OAM_{0}^{-}	OAM_{-1}^{-}	OAM_{-2}^{-}	OAM_{-3}^{-}	OAM_{-4}^{-}	OAM_{-5}^{-}
137 rad/m	134 rad/m	129 rad/m	122 rad/m	113 rad/m	105 rad/m

shows that when the twist rate is in the range of 21 to 38 rad m^{-1}, all effective refractive index differences are greater than 10^{-4} as shown in Fig. 4(c). When the twist rate is 33 rad m^{-1}, the minimum effective refractive index difference of the 22 modes is 1.66×10^{-4}. Therefore, the optimal twist rate of this fiber is 33 rad m^{-1}. Such a twist rate is relatively easy to implement in practical applications. In contrast, the optimal twist rate of the twisted air-hole ring-core fiber mentioned in the literature study [18] is 381 rad m^{-1}, which is too high to be applied in practice.

At the optimal twist rate of 33 rad m^{-1}, and the operating wavelength of 1.55 μm, the number of modes supported by the fiber at different radii and the minimum mode separation were calculated, as presented in the following Table:

Fiber core radius	1.3	2.0	2.7	2.9	4.0	5.0
Number of supported modes	2	6	10	14	18	22
Minimum mode separation	2.9912 $\times 10^{-4}$	3.1130 $\times 10^{-4}$	2.3298 $\times 10^{-4}$	1.4475 $\times 10^{-4}$	1.3629 $\times 10^{-4}$	1.8137 $\times 10^{-4}$

3.3 The Effective Mode Field of the Fiber

The effective mode field area, A_{eff}, can be used to quantitatively measure the transverse area occupied by a certain mode. It is given by the following expression [25]

$$A_{eff} = \frac{\left(\iint \left|E^2\right| dxdy\right)^2}{\iint \left|E^4\right| dxdy} \tag{4}$$

where E denotes the transverse electric field on the cross section of the fiber. A large effective mode field area can effectively increase the damage threshold and increase the transmission power of the fiber. Fig. 6(a) demonstrates that the mode field area of a mode in a twisted inverse-parabolic fiber changes with wavelength. The effective mode field area of different modes increases with wavelength, and gradually decreases with topological charge. Owing to structural differences, the effective mode field area of the twisted air-hole ring-core fiber increases with topological charge of the mode; however, it is smaller than the mode field area of the corresponding mode in the twisted inverse-parabolic fiber [19]. At a wavelength of 1.55 μm, the effective mode field area of a mode

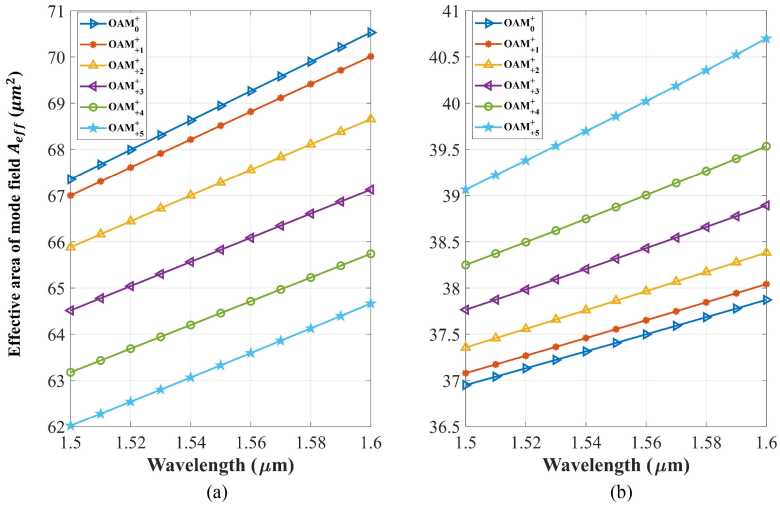

Fig. 6. The effective area of mode field: (a) the twisted inverse-parabolic fiber and (b) the twisted air-hole ring-core fiber.

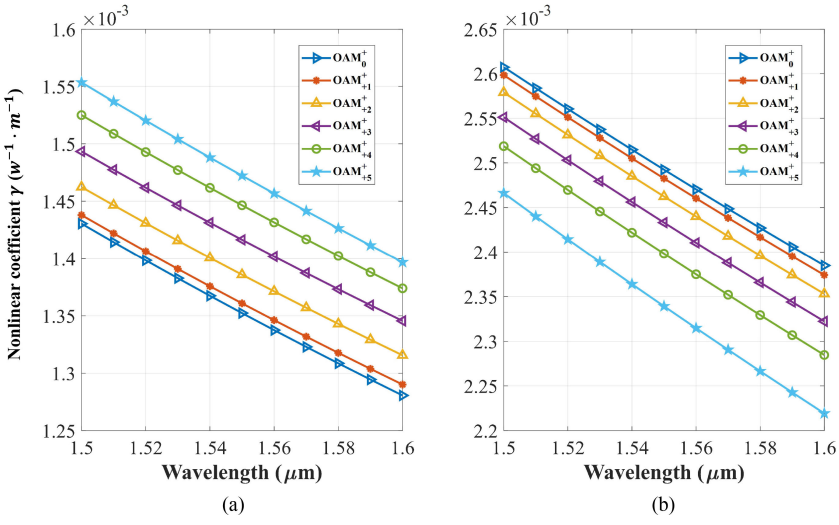

Fig. 7. The nonlinear coefficient of modes: (a) the twisted anti-parabolic fiber and (b) the twisted air-hole ring-core fiber.

with topological charge 0 in a twisted inverse-parabolic fiber is 68.94 μm^2, and the area of the corresponding mode in the twisted air-hole ring-core fiber is 37.31 μm^2.

3.4 The Nonlinearity of the Fiber

The nonlinearity of a light wave propagating in an optical fiber, γ, is unfavorable. Under the same optical power, the magnitude of the nonlinearity is proportional to the nonlinear refractive index, n, and inversely proportional to the effective area of the mode field, as shown in the following expression [25]

$$\gamma = \frac{2\pi}{\lambda} \frac{n}{A_{eff}} \tag{5}$$

Figs. 7(a) and (b) show the nonlinear coefficients of the twisted inverse-parabolic fiber and the ring-core air-hole fiber mode, respectively. The nonlinear coefficients of both are around 10^{-3} w^{-1} m^{-1}, but all the nonlinear coefficients of the former are smaller than those of the latter.

4. Conclusions

In this study, the eigenstates of an inverse-parabolic fiber under torsional stress were studied, and the simulation results showed that the separation of the 22 eigenmodes in the vortex state of the fiber under low torsional stress satisfies both wavelength division multiplexing and mode division multiplexing over the entire C-band wavelengths. This way of generating vortices does not require the superposition of eigenstates. The optimal twisted rate required by this fiber is an order of magnitude smaller than that required by the torsional air-hole ring-core fiber. Moreover, it has larger mode field area and smaller nonlinearity.

References

[1] R. J. Essiambre and R. W. Tkach, "Capacity trends and limits of optical communication networks," in *Proc. IEEE*, vol. 100, no. 5, pp. 1035–1055, 2012.
[2] D. J. Richardson, J. M. Fini, and L. E. Nelson, "Space-division multiplexing in optical fibres," *Nat Photon*, vol. 7, no. 5, pp. 354–362, 05//print, 2013.
[3] N. Bozinovic *et al.*, "Terabit-scale orbital angular momentum mode division multiplexing in fibers," *Science*, vol. 340, no. 6140, pp. 1545–1548, 2013.
[4] J. Wang, "Advances in communications using optical vortices," *Photon. Res.*, vol. 4, no. 5, 2016.
[5] J. Wang *et al.*, "Terabit free-space data transmission employing orbital angular momentum multiplexing," *Nat Photon*, vol. 6, no. 7, pp. 488–496, 07//print, 2012.
[6] M. Dienerowitz, M. Mazilu, P. J. Reece, T. F. Krauss, and K. Dholakia, "Optical vortex trap for resonant confinement of metal nanoparticles," *Opt. Express*, vol. 16, no. 7, pp. 4991–4999, 2008.
[7] J. Ng, Z. Lin, and C. Chan, "Theory of optical trapping by an optical vortex beam," *Physical Rev. Lett.*, vol. 104, no. 10, pp. 103601, 2010.
[8] G. Molina-Terriza, J. P. Torres, and L. Torner, "Twisted photons," *Nature Phys.*, vol. 3, no. 5, pp. 305, 2007.
[9] G. Gibson *et al.*, "Free-space information transfer using light beams carrying orbital angular momentum," *Opt. Express*, vol. 12, no. 22, pp. 5448–5456, 2004.
[10] T. A. F. A. N. Alexeyev and A. V. Volyar, "Optical vortices and the flow of their angular momentum in a multimode fiber," *Semicond. Phys., Quantum Electron. Optoelectronics.*, vol. V1, no. N1, pp. 82–89, 1998.
[11] S. Ramachandran, P. Kristensen, and M. F. Yan, "Generation and propagation of radially polarized beams in optical fibers," *Opt. Lett.*, vol. 34, no. 16, pp. 2525–2527, 2009/08/15.
[12] P. Gregg, P. Kristensen, S. Golowich, J. Olsen, P. Steinvurzel, and S. Ramachandran, "Stable transmission of 12 OAM states in air-core fiber," in *Proc. OSA Tech. Dig. (online)*. p. CTu2K.2.
[13] B. Ung *et al.*, "Inverse-parabolic graded-index profile for transmission of cylindrical vector modes in optical fibers," in *Proc. OSA Tech. Dig. (online)*. p. Tu3K.4.
[14] Y. Yue *et al.*, "Octave-spanning supercontinuum generation of vortices in an As 2 S 3 ring photonic crystal fiber," *Opt. Lett.*, vol. 37, no. 11, pp. 1889–1891, 2012/06/01.
[15] G. Zhou, G. Zhou, C. Chen, M. Xu, C. Xia, and Z. Hou, "Design and analysis of a microstructure ring fiber for orbital angular momentum transmission," *IEEE Photon. J.*, vol. 8, no. 2, 2016, Art. no. 7802512.
[16] R. Bhandari, "Orbital angular momentum (OAM) mode mixing in a bent step index fiber in perturbation theory: Multiple bends," *IEEE Photon. J.* vol. 11, no. 3, Jun. 2019, Art. no. 7200510.
[17] L. Wang and S. LaRochelle, "Design of eight-mode polarization-maintaining few-mode fiber for multiple-input multiple-output-free spatial division multiplexing," *Opt. Lett.* vol. 40, pp. 5846–5849, 2015.
[18] S. Ramachandran and P. Kristensen, "Optical vortices in fiber," *Nanophotonics*, vol. 5-6, p. 455, 2013.
[19] J. Ye, *et al.*, "Excitation and separation of vortex modes in twisted air-core fiber," *Opt. Express*, vol. 24, no. 8, pp. 8310–6, Apr. 18, 2016.
[20] B. Ung, P. Vaity, L. Wang, Y. Messaddeq, L. A. Rusch, and S. LaRochelle, "Few-mode fiber with inverse-parabolic graded-index profile for transmission of OAM-carrying modes," *Opt. Express*, vol. 22, no. 15, pp. 18044–18055, 2014/07/28.
[21] A. Nicolet, F. Zolla, Y. Ould Agha, and S. Guenneau, "Geometrical transformations and equivalent materials in computational electromagnetism," *COMPEL-The Int. J. Comput. Math. Elect. Electron. Eng.*, vol. 27, no. 4, pp. 806–819, 2008.
[22] A. Nicolet, F. Zolla, and S. Guenneau, "Modelling of twisted optical waveguides with edge elements," *Eur. Physical J. Appl. Phys.*, vol. 28, no. 2, pp. 153–157, 2004.
[23] X. Ma, C.-H. Liu, G. Chang, and A. Galvanauskas, "Angular-momentum coupled optical waves in chirally-coupled-core fibers," *Opt. Express*, vol. 19, no. 27, pp. 26515–26528, 2011/12/19.
[24] C. Brunet, P. Vaity, Y. Messaddeq, S. LaRochelle, and L. A. Rusch, "Design, fabrication and validation of an OAM fiber supporting 36 states," *Opt. Express*, vol. 22, no. 21, pp. 26117–26127, 2014/10/20.
[25] G. Agrawal, "Nonlinear fiber optics," vol. 160, no. 18, pp. 1–1, 2001.